J. Indian Inst. Sci.
A Multidisciplinary Reviews Journal
ISSN: 0970-4140 Coden-JIISAD

REVIEW ARTICLE

Modeling and Simulation of Dropwise Condensation: A Review

Manjinder Singh[1†], Nilesh D. Pawar[1†], Sasidhar Kondaraju[2] and Supreet Singh Bahga[1]*

Abstract | In this review, we present significant developments that have been made in the mathematical modeling and simulations of dropwise condensation. In dropwise condensation, vapor condenses in the form of distinct drops. Modeling of DWC involves modeling heat transfer through a single drop and applying it to a population of drops. In the first part, we discuss heat transfer through a single droplet and compare the approximate analytical solution with the results of numerical simulations. We also address the shortcomings of the analytical model. In the second part, we present methods utilized to find the drop size distribution which are coupled with a model for heat transfer through the single droplet to obtain overall dropwise condensation heat transfer rate. In particular, we discuss the population balance method and the Monte Carlo method to predict drop size distribution and heat transfer rate. We support our discussion with the results from the literature.

Keywords: *Droplet growth, Population balance method, Monte Carlo simulations*

1 Introduction

Condensation of vapor plays a crucial role in a wide range of large-scale energy systems. In particular, steam power plants and HVAC systems, which, respectively, account for 78% of global electric power generation[1, 2] and 10–20% of total energy consumption in developed countries[3], rely on the process of vapor condensation. Besides steam power plants and HVAC systems, efficiency of several industrial applications such as water desalination[4–7], water collection[8–10] and thermal management[11–13] depend on vapor condensation. Therefore, any improvement in the efficiency of vapor condensation process can lead to significant energy savings.

Condensation can be categorized as either filmwise condensation (FWC) or dropwise condensation (DWC). Figure 1 shows the schematic and Fig. 2 shows the images illustrating FWC and DWC. In FWC, the condensate forms a liquid film on the surface. This liquid film provides additional thermal resistance to heat transfer between the surface and the vapor. On the other hand, in DWC, vapor forms distinct liquid drops with dimensions ranging from ($\sim 10 - 200$ nm) on the nucleation sites[14, 15]. These liquid drops grow, coalesce with neighboring drops and roll off the surface due to gravity (known as droplet shedding) as shown in Fig 1b. The rolling droplets remove other droplets in their path and clear the surface for re-nucleation. As the drops have a higher surface area than the liquid film, these continuous cycles of drop nucleation, growth, coalescence, and departure from the surface result in order of magnitude higher heat transfer coefficients in DWC compared to FWC[16–18]. However, ideal DWC occurs only at low values of temperature difference ΔT (termed as the degree of subcooling) between a surface and saturated vapor. As the degree of subcooling is progressively increased, condensation first transitions to mixed mode consisting of partial DWC and partial FWC. At sufficiently high values of degree of subcooling, condensation becomes completely filmwise[18–20]. Typically, removal of drops in DWC occurs due to gravity. However, condensate drop can also be removed using a surface with wettability gradient[21–24]. Figure 3 shows the DWC on

Manjinder Singh, Nilesh D. Pawar contributed equally to this work.

[1] Department of Mechanical Engineering, Indian Institute of Technology Delhi, Hauz Khas, New Delhi 110016, India.
[2] School of Mechanical Sciences, Indian Institute of Technology Bhubaneswar, Khurda 752050, Odisha, India.
**bahga@mech.iitd.ac.in*

Springer IISc Press

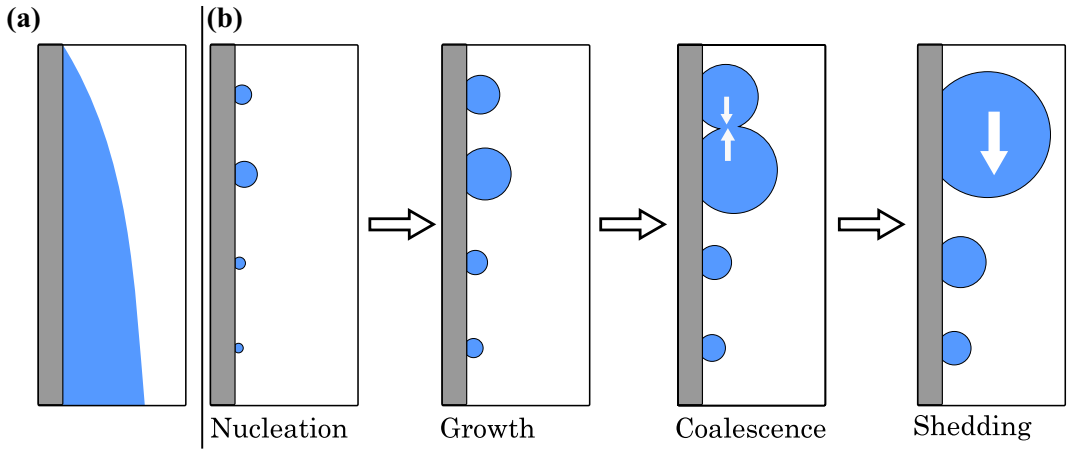

Figure 1: Schematic illustrating different modes of condensation. **a** Filmwise condensation, **b** dropwise condensation.

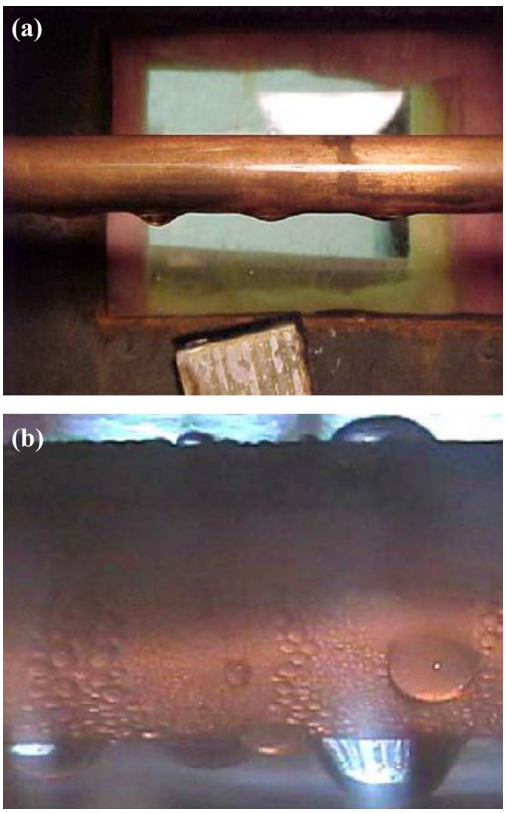

Figure 2: Images showing **a** filmwise condensation and **b** dropwise condensation on a cylindrical pipe. Reprinted from Vemuri et al.[25] Copyright 2005, with permission from Elsevier.

a surface with wettability gradient. On surfaces with wettability gradient, the drops condense and migrate towards the more wetting region.

Dropwise condensation has been a focus of several extensive reviews, including those by Rose[18], Enright et al.[26], Cho et al.[27], and Wen et al.[14]. Rose[18] presented a review of measurements of heat transfer, the transition from DWC to FWC, and the effects of condensing surface material. The review article of Enright et al.[26] discussed developments of fabrication methods to create micro- and nanoscale structures to make surfaces superhydrophobic. Cho et al.[27] presented a review on nanoengineered and mixed-wettability surface for liquid–vapor phase change heat transfer. Recently, in a related review article, Wen et al.[14] discussed functionalized nanowired surfaces for phase change heat transfer and their fabrication techniques. Here, we present a systematic review of modeling and simulation methods employed to study dropwise condensation.

The classification of various modeling and simulation techniques for DWC is shown in Fig 4. Modeling of DWC involves modeling heat transfer through a single drop and applying it to a population of drops. We begin by reviewing the mathematical models and simulation studies of heat transfer through a single condensing droplet. We then present the growth dynamics of multiple droplets during condensation. In particular, we present a mathematical approach to couple heat transfer through a single droplet and the drop size distribution. Thereafter, we discuss different strategies for obtaining the drop size distribution using population balance method and Monte Carlo simulations. We note that unless specified otherwise the results reported in this review article is for water as working fluid.

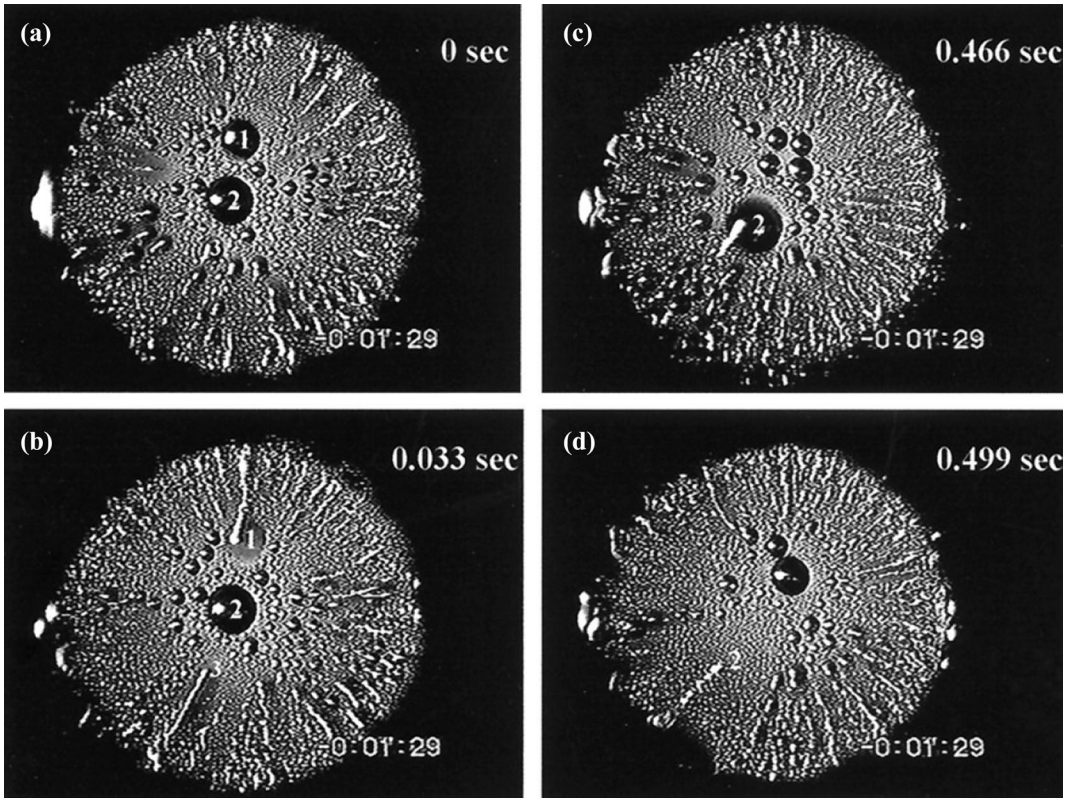

Figure 3: Dropwise condensation on a disk-shaped horizontal surface with wettability gradient[21]. The wettability of the surface increases from center to periphery which causes spontaneous motion of the condensed water drops. Reprinted from Daniel et al.[21] Copyright 2001, with permission from AAAS.

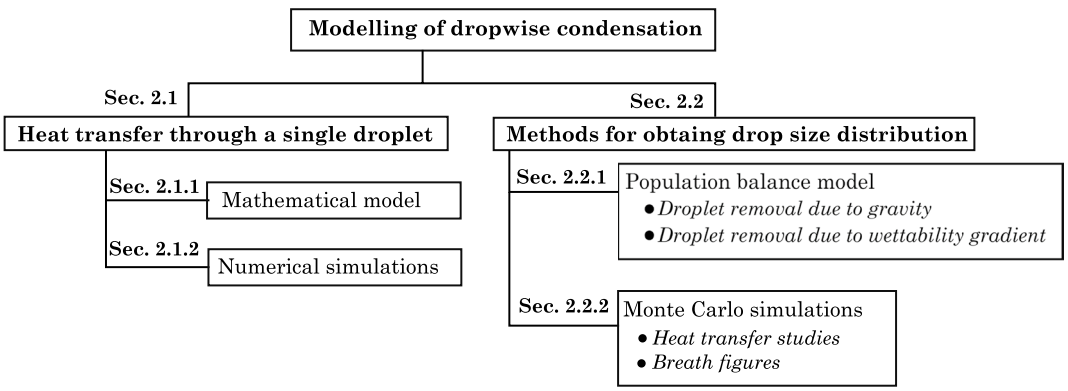

Figure 4: Classification of various modeling and simulation methods for dropwise condensation.

2 Modeling of Dropwise Condensation

Due to inherent unsteady behavior of dropwise condensation, investigators have used a statistical approach to model the dropwise condensation heat transfer[18, 28, 29]. The statistical approach is based on the experimental observation that although individual drop growth is unsteady, the overall drop size distribution remains constant with time. Figure 5 shows a typical drop size distribution in DWC consisting of small drops and large drops. Small drops are those that grow mainly by direct condensation of vapor, whereas large drops grow mainly by coalescence with other drops. In the statistical approach, heat transfer through a drop of given radius is multiplied with its respective population density and then integrated over the entire drop size

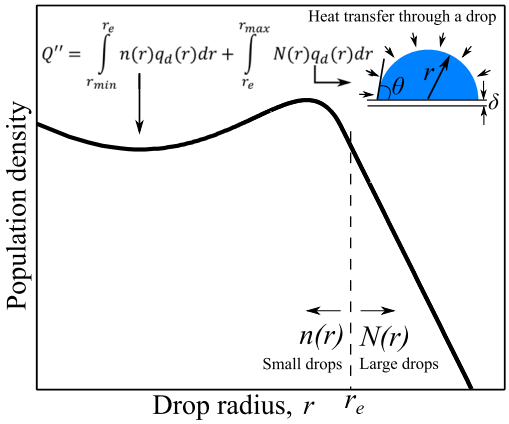

Figure 5: Schematic showing a typical drop size distribution in dropwise condensation. Condensed droplets are categorized as (i) small drops $n(r)$ that grow primarily by direct condensation and (ii) large drops $N(r)$ that grow by coalescence with other drops Reprinted from Singh et al.[24] Copyright 2018.

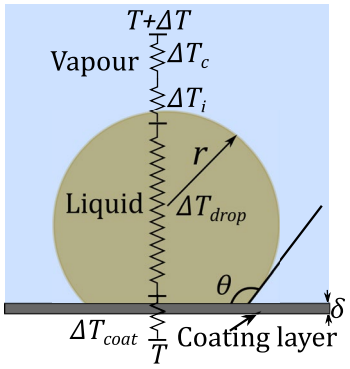

Figure 6: Schematic showing temperature drop due to various resistances to heat transfer through a drop in a condensation environment. The temperature drop ΔT_c is due to curvature resistance, ΔT_i represents temperature drop due to liquid–vapor interfacial resistance, ΔT_{drop} denotes temperature drop due to drop itself and ΔT_{coat} is temperature drop due to coating layer.

distribution to obtain the overall condensation heat transfer rate Q'' as

$$Q'' = \int_{r_{min}}^{r_e} q_d(r)\, n(r)\, dr + \int_{r_e}^{r_{max}} q_d(r)\, N(r)\, dr. \quad (1)$$

Here, $n(r)$ and $N(r)$, respectively, are number of small and large drops per unit area per unit radius around r. The radius r_e, as shown in the Fig. 5, denotes drop radius at the boundary between small and large drops and q_d denotes heat transfer through a drop of radius r. In Eq. (1) r_{min} is the minimum viable drop radius given by[30]

$$r_{min} = \frac{2T_{sat}\gamma}{h_{fg}\rho\Delta T}. \quad (2)$$

Drops smaller than size r_{min} are not stable due to high pressure. For example, pressure inside the drop of radius 10 nm is 10^2 atm higher than pressure inside the drop of size 1 μ m. Therefore, small drops ($< r_{min}$) either disintegrate or fuse to form a larger drop. In Eq. (2) ΔT is the degree of subcooling, that is the temperature difference between vapor and condensation surface, γ is the surface tension of the liquid, ρ is the density of liquid, T_{sat} is the saturation temperature and h_{fg} is the latent heat of condensation. First, we will describe the methods for obtaining heat transfer through a single droplet which will be followed by methods used for obtaining drop size distribution.

2.1 Methods for Obtaining Heat Transfer Through A Single Droplet

The first step in modeling DWC is to estimate heat transfer through a single drop. The heat transfer through a single droplet is either found through (i) an approximate analytical model or (ii) by numerical simulations.

2.1.1 Mathematical Model

The analytical model for rate of heat transfer through a drop of given radius r was first presented by LeFevre and Rose[31]. Figure 6 shows the temperature drop due to various resistances to heat transfer in dropwise condensation. In their model, LeFevre and Rose considered liquid–vapor interfacial resistance, conduction resistance due to drop itself, resistance of coating layer and resistance due to curvature of the liquid–vapor interface. They assumed that within the drop, convection is negligible and conduction is the dominant heat transfer mechanism. However, the model considered all the drops to be hemisphere with a contact angle of 90°. Kim and Kim[29] improved the model of LeFevre and Rose to include the heat transfer through drops of all contact angle. In particular, Kim and Kim modeled the temperature drop due to conduction resistance. To model the conduction heat transfer within the drop, Kim and Kim considered the drop to be made up of a large number of isotherms each separated by an infinitesimal distance.

The temperature drop due to conduction is obtained by integrating temperature drop across all the isotherms. For a drop of radius, r and contact angle, θ on a plain surface with coating layer of thickness, δ the temperature drop due to resistance to conduction of heat by the drop itself is given by

$$\Delta T_{\text{drop}} = \frac{q_{\text{d}}\theta}{4\pi r K_{\text{c}} \sin\,\theta}, \tag{3}$$

where q_{d} is the rate of heat transfer and K_{c} is the thermal conductivity of the water. The temperature drop due to interfacial resistance, ΔT_{i} is expressed as

$$\Delta T_{\text{i}} = \frac{q_{\text{d}}}{h_{\text{i}} 2\pi r^2 (1 - \cos\theta)}, \tag{4}$$

where h_{i} is the heat transfer coefficient. The temperature drop due to coating layer, ΔT_{coat} and curvature of the drop, ΔT_{c} are, respectively, expressed as

$$\Delta T_{\text{coat}} = \frac{q_{\text{d}}\delta}{K_{\text{coat}}\pi r^2 \sin^2\theta}, \tag{5}$$

$$\Delta T_{\text{c}} = \frac{r_{\min}}{r}\Delta T, \tag{6}$$

where K_{coat} represents the thermal conductivity of the coating layer. Adding temperature drop due to all the resistances and rearranging gives the heat transfer rate through a single drop of radius r as

$$q_{\text{d}} = \frac{\Delta T \pi r^2 \left(1 - \frac{r_{\min}}{r}\right)}{\frac{\delta}{K_{\text{coat}} \sin^2\theta} + \frac{r\theta}{4K_{\text{c}} \sin\theta} + \frac{1}{2h_{\text{i}}(1 - \cos\theta)}}. \tag{7}$$

Equation (7) shows that the rate of heat transfer through a drop of radius r depends on the solid–liquid contact angle. Figure 3 of reference[29] shows the effect of contact angle on heat transfer through a drop. For contact angles greater than 90°, the rate of heat transfer through a single drop decreases with an increase in contact angle. However, the corresponding heat flux increases with an increase in contact angle. This difference in the variation of the rate of heat transfer and heat flux with an increase in contact angle is attributed to the increase in conduction resistance of drops with an increase in contact angle. However, decreasing the base area of the drop with increasing contact angle results in higher heat flux.

2.1.2 Numerical Simulations of Heat Transfer Through a Single Drop

The approximate analytical model discussed in Sect. 2.1.1 is based on the assumption that the temperature of the liquid–vapor interface is constant and is equal to the saturation temperature of vapor T_{s}. In addition to constant interface temperature, the analytical model neglects the effect of convection and assumes the dominant mode of heat transfer through the droplet is conduction because of the sufficiently small size droplets. However, convection inside the droplet can occur due to buoyancy and Marangoni effects[32]. Marangoni effects is fluid flow due to gradient in surface tension of the fluid caused by temperature gradient. Guadarrama-Cetina et al.[33] presented a scaling analysis to show that fluid flow due to buoyancy effects is negligible in dropwise condensation. However, the convection can be significant due to the Marangoni effect under a wide range of conditions.

Recently, significant improvements have been made to simulate the heat transfer through a single droplet, beginning with the work of Chavan et al.[34]. Chavan et al. developed a steady-state two-dimensional axisymmetric simulation method for an individual droplet growth on non-wetting surfaces ($90° < \theta < 170°$). In their model, the simplifying assumption of constant liquid–vapor interface temperature which was previously used in the analytical model is replaced by a convective boundary condition with constant heat transfer coefficient h_{i}. These simulations showed that the temperature variation and thus, heat flux variation are significant near the three-phase contact line. In addition, these quantities are dependent on the droplet size R_{b} which is expressed in terms of non-dimensional Biot number $Bi = h_{\text{i}}R_{\text{b}}/k_{\text{w}}$, where k_{w} is the thermal conductivity of liquid. When the heat transfer from the simulation is combined with drop size distribution, the analytical model, given by Eq. (7), underpredicts the total heat transfer nearly 300% as shown in Fig. 7. This is because the analytical model fails to predict the local heat transfer at the three-phase contact line. Later, in a related publication, Phadnis and Rykaczewski[35] extended the model of Chavan et al.[34] to account for the effect of Marangoni convection. Phadnis and Rykaczewski found a sixfold increase in the heat transfer compared to pure conduction case on the superhydrophobic surface for large droplets ($\sim$ 1 mm) under extreme subcooling (50 K) as shown in Fig 8. However, the total heat transfer obtained by combining individual drop heat transfer with drop size distribution gives 10%

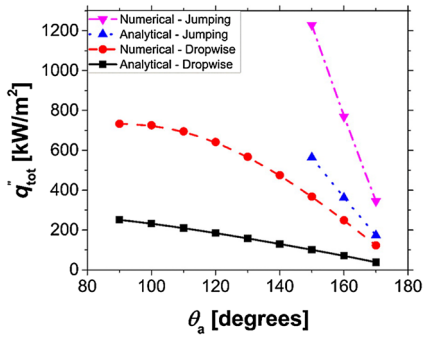

Figure 7: Comparison of the variation of total heat flux estimated using a mathematical model and numerical simulations with the contact angle of the surface. The analytical model under predicts the overall heat transfer nearly 300% compared to the numerical simulations. This is because the approximate analytical model fails to predict the local heat transfer at the three-phase contact line. Reprinted with permission from Chavan et al.[34]. Copyright 2016, American Chemical Society.

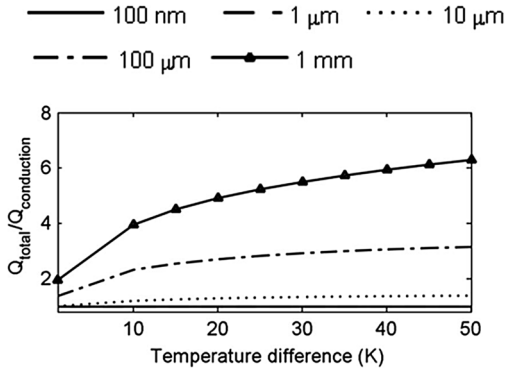

Figure 8: The ratio of heat transfer with Marangoni convection Q_{total} and with pure conduction $Q_{conduction}$ for a surface with 150° contact angle for different droplet sizes. Reprinted from Phadnis and Rykaczewski[35]. Copyright 2017, with permission from Elsevier.

or lower enhancement over a stationary drop. Therefore, Phadnis and Rykaczewski proposed the use of a classical mathematical model with the convective boundary condition at the liquid–vapor interface as suggested by Chavan et al.

The analytical model and above numerical studies are based on the assumption of quasi-steady-state heat conduction through the droplet because the conduction time scale, $\tau_{\text{conduction}} = r^2/\alpha \approx 7\,\mu\text{s}$ (α is the thermal diffusivity) is much smaller compared with the droplet growth time scale $\tau_{\text{growth}} \approx 1$ ms[36]. However, the droplet growth process is inherently transient and the steady state is never reached[37]. Moreover, the droplet grows from nucleation size ($\sim 10 - 200$ nm) to hundreds of micrometer[14]. Therefore, the droplet growth process is dynamic and multiscale. Xu et al.[37] presented a multiscale growth model that coupled the transient two-phase heat transfer with two-phase fluid flow. The heat transfer between the two phases of the fluid is governed by the energy equation given by

$$\rho c_{\text{p}} \frac{\partial T}{\partial t} + \rho c_{\text{p}} (\mathbf{u} \cdot \nabla T) = \nabla \cdot (k \nabla T), \tag{8}$$

where c_{p} is the specific heat capacity, and k is the thermal conductivity. The flow velocity $\mathbf{u}$ is determined by solving the continuity equation

$$\nabla \times \mathbf{u} = 0 \tag{9}$$

and Navier–Stokes equation

$$\rho \frac{\partial \mathbf{u}}{\partial t} + \rho(\mathbf{u} \cdot \nabla)\mathbf{u} = -\nabla \mathbf{p} + \mu \nabla^2 \mathbf{u} + \rho \mathbf{g}. \tag{10}$$

where p is pressure and g is acceleration due to gravity. Figure 9 shows the schematic illustrating multiscale droplet growth model. As the drop grows due to vapor condensation, the liquid–vapor interface expands and so does the three-phase contact line, as shown in Fig. 9. To allow for the motion of three-phase contact line, Eqs. (9) and (10) are solved using Navier-slip boundary condition.

Figure 10 shows the comparison of predictions of multiscale model, pure conduction model, and static convection model for droplet sizes from 50 nm to 500 μm. Xu et al.[37] described the droplet growth process in three stages based on droplet size R: (i) conduction dominated ($< 5\,\mu$m), (ii) transient ($\sim 5 - 200\,\mu$m), where convection is attributed to coupled effect of Marangoni flow and interfacial mass flow, and (iii) convection dominated ($> 200\,\mu$m), which is completely characterized by interfacial mass flow-induced convection. In addition, this model showed a fourfold increase in heat transfer of an individual droplet compared with the analytical model discussed in Sect. 2.1.1. However, they did not report details of the overall heat transfer from the surface.

2.2 Methods for Obtaining Drop Size Distribution

After obtaining the rate of heat transfer through a drop of radius r from either of the above-mentioned approaches, the next step is to find the

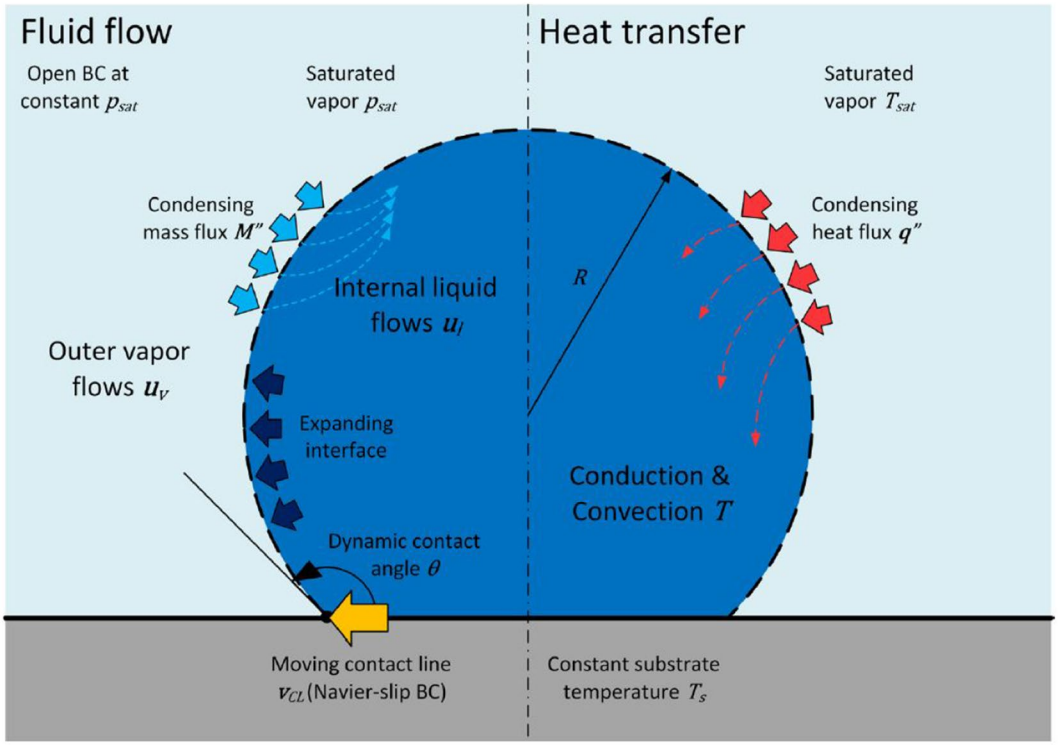

Figure 9: Schematic illustrating multiscale droplet growth model that coupled the transient two-phase heat transfer with two-phase fluid flow. Right side of the schematic shows the transient two-phase heat transfer which is solved using the energy equation. The droplet is placed on a surface having temperature T_s. The latent heat given up by vapor enters the drop through the liquid–vapor interface. The left side of the schematic shows the transient fluid flow within the drop. The flow velocity **u** is obtained by solving the Navier–Stokes equation using Navier-slip boundary condition to allow for the motion of three-phase contact line. Reprinted with permission from Xu et al.[37]. Copyright 2018, American Chemical Society.

corresponding drop population. In this section, we describe the different approaches employed to obtain the drop size distribution in DWC. Once the distribution of drop size is known, the total heat transfer can be obtained using Eq. (1).

2.2.1 Population Balance Model

Various analytical approaches[28,31] have been used to find the drop population, however, the population balance model proposed by Maa[38] and later improved by Abu-Orabi[39] is by far the most widely used and gives more accurate predictions than any other model. In the population balance model, drops are categorized into small drops and large drops based on growth mechanism. As mentioned in Sect. 2, small drops are those that grow mainly by direct condensation of vapor on drop surface. On the other hand, large drops grow mainly by coalescence with other drops. The drop size distribution of large drops is obtained using the empirical relation given by LeFevre and Rose[31]. To obtain the drop size distribution of small drops, the model uses the method of population balance that is drop population in a given radius range is conserved. Consider an arbitrary droplet radius range, $r_1 - r_2$. In the population balance approach, the number of drops that grow into $r_1 - to - r_2$ due to condensation is equal to the sum of drops that grow out of the radius range and those swept by large drops departing from condensation surface.

If n_1 and n_2 denote population density of drops of radius r_1 and r_2, respectively, then the number of drops entering the radius range $r_1 - r_2$ by growth in differential time increment dt can be expressed as $An_1G_1\mathrm{d}t$, where G denotes the droplet growth rate and A is the area of condensing surface. Similarly, the number of drops leaving this radius range by growth is $An_2G_2\mathrm{d}t$. When large drops move under the influence of external force, some of the drops in $r_1 - r_2$ radius range get swept along with them. The number of drops removed due to this sweeping effect is given by $Sn_{1-2}\Delta rdt$, where S is the surface renewal rate

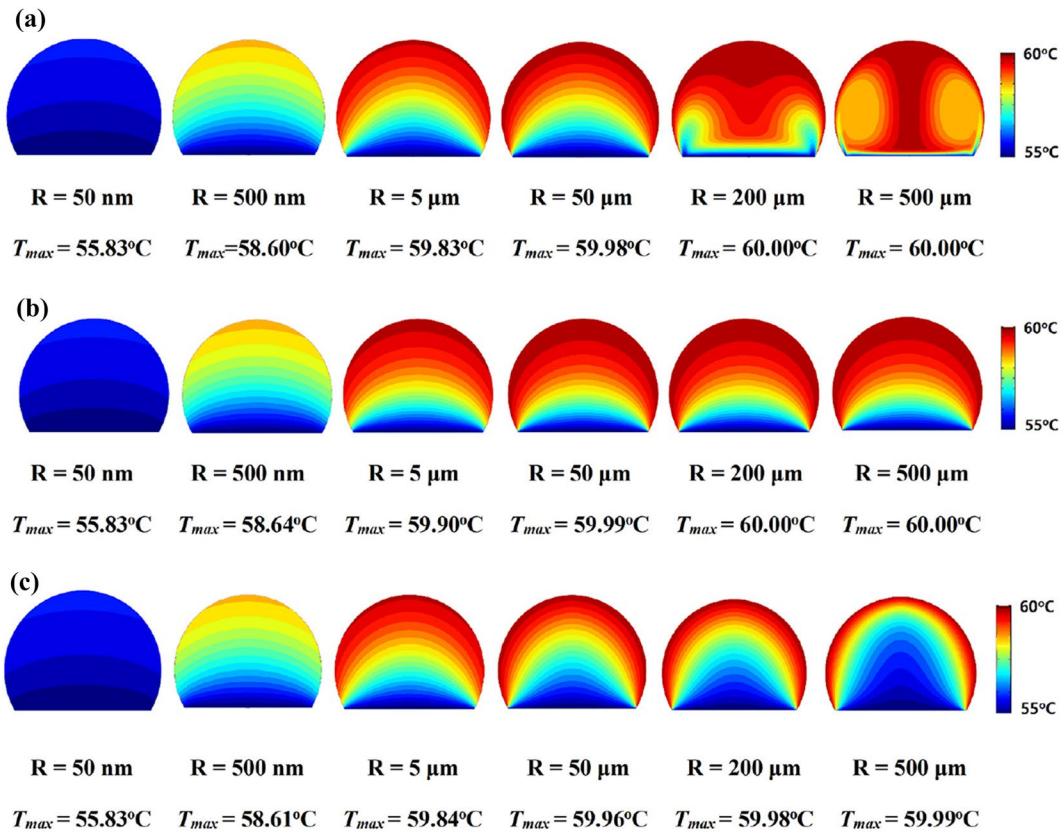

Figure 10: Comparison of temperature distribution inside a droplet for sizes from 50 nm to 500 µm. **a** Multiscale dynamic growth model, **b** pure conduction, and (c) static convection model. Reprinted with permission from Xu et al.[37]. Copyright 2018, American Chemical Society.

due to sweeping effect, n_{1-2} is the mean population density in the $r_1 - r_2$ radius range and $\Delta r = r_2 r_1$. For the population of the drops to be conserved in this radius range, we must have

$$An_1 G_1 \mathrm{d}t = An_2 G_2 \mathrm{d}t + Sn_{1-2}\Delta r \mathrm{d}t. \tag{11}$$

Equation (11) can be further simplified to

$$A(G_1 n_1 - G_2 n_2) = Sn_{1-2}\Delta r. \tag{12}$$

As Δr approaches zero, n_{1-2} becomes a point value and Eq. (12) can now be expressed as ,

$$\frac{\mathrm{d}}{\mathrm{d}r}(Gn) + \frac{n}{\tau} = 0, \tag{13}$$

where $\tau = A/S$ is the sweeping period. In Eq. (13), the droplet growth rate G is one of the unknown parameters. To obtain G, the heat transfer rate through a drop of radius r is equated to the condensation rate of vapor at the drop surface, even though the size of drop changes during heat transfer due to simultaneous condensation of vapor. This acceptable because the time scale of conduction heat transfer is very small ($\sim 1\,\mu$s) compared to the time scale of droplet growth (~ 1 ms) and therefore conduction heat transfer through the drop of radius r can be treated as a quasi-steady process. That is, drop size can be assumed to be constant during the conduction heat transfer. Also, there is no direct heat transfer between vapor and condensation surface, and all the heat transfer occurs through the drops. Using the quasi-steady heat conduction approximation G is expressed as

$$G = \frac{q_{\mathrm{d}}}{\rho h_{fg} 2\pi r^2 (1 - \cos\,\theta)}. \tag{14}$$

Next, the expression for G is used in Eq. (13) and integrated to get the drop size distribution of small drops. The constant of integration is obtained using the boundary conditions that at the drop radius at which drop growth by coalescence begins to dominate drop growth due to direct condensation $n(r_{\mathrm{e}}) = N(r_{\mathrm{e}})$. Here $N(r)$ denotes drop size distribution of large drops. The drops are classified as large drops if they grow mainly due to coalescence with other drops. The drop size distribution of large is given by the empirical relation of LeFevre and Rose[31] expressed as

$$N(r) = \frac{1}{3\pi r^2 r_{\max}} \left(\frac{r}{r_{\max}} \right)^{-2/3}. \quad (15)$$

Here, $r_{\max}$ is the drop radius at which drops spontaneously depart from the condensation surface and is an unknown parameter.

While the radius of smallest drop ($r_{\min}$) is obtained from thermodynamic limit (Eq. (2)), the radius of largest drop depends on the force responsible for affecting droplet departure from condensation surface. Correct estimation of largest drop size is obtained by equating the force trying to remove the droplet from condensation surface with force resisting the droplet removal. Typically, the force resisting the droplet removal is hysteresis force. Whereas, there are different types of forces affecting spontaneous removal of drops including gravity and force due to wettability gradient.

Droplet removal due to gravity In majority of applications of dropwise condensation, condensed drops are removed due to gravity. The gravity is used for droplet removal by inclining the condensation surface. The hysteresis force that resists the drop removal is given by[40]

$$F_{\text{hys}} = 2r \sin\theta \sigma (\cos\theta_{\text{r}} - \cos\theta_{\text{a}}), \quad (16)$$

where subscripts r and a, respectively, denote receding and advancing contact angles. The gravitational force on the drop is given by

$$F_{\text{g}} = \frac{\pi r^3 \rho g}{3} (2 - 3\cos\theta + \cos^3\theta). \quad (17)$$

Equating the gravitational force with hysteresis force gives the drop departure radius as[29]

$$r_{\max} = \left(\frac{6 \sin\theta \sigma (\cos\theta_r - \cos\theta_a)}{\pi \rho g (2 - 3\cos\theta + \cos^3\theta)} \right). \quad (18)$$

Substituting $r_{\max}$ in Eq. (15) gives the drop departure radius which in turn gives the drop size distribution of large drops. Next, the boundary radius r_e between large and small drops is obtained by assuming that nucleation sites have a uniform distribution over the surface and form a square array which gives r_{e}. Once r_{e} is known, then the integration constant obtained after the integration of Eq. (13) is found using the boundary condition $n(r_{\text{e}}) = N(r_{\text{e}})$ and the drop distribution of small drops is expressed as

$$n(r) = \frac{1}{3\pi {r_e}^3 r_{\max}} \left(\frac{r_{\max}}{r_{\text{e}}} \right)^{2/3} \frac{r}{C} \frac{A_2 r + A_3}{A_2 r_e + A_3} \exp(B), \quad (19)$$

where

$$B = \frac{A_2}{\tau A_1} \left[\frac{{r_e}^2 - r^2}{2} + r_{\min} C - {r_{min}}^2 \ln D \right] + \frac{A_3}{\tau A_1} \left[C - r_{\min} \ln D \right], \quad (20)$$

$C = r_e - r$, $D = (r - r_{\min})/(r_e - r_{\min})$, $A_1 = \Delta T / 2\rho h_{fg}$, $A_2 = \theta(1 - \cos\theta)/4K_c$ and $A_3 = \delta(1 - \cos\theta)/(K_{coat} \sin^2\theta) + 1/h_i$. The unknown factor τ is obtained using the condition that[28,39]

$$\frac{\mathrm{d}(\ln n(r))}{d(\ln r)} = \frac{\mathrm{d}(\ln N(r))}{d(\ln r)} = -\frac{8}{3}. \quad (21)$$

Kim and Kim[29] validated their mathematical model with the experimental results of Vemuri and Kim[41] and Vemuri et al.[25] (see Fig. 6 of reference[29]). The mathematical model for DWC agrees well with experimental results for the degree of subcooling less than 3 K, at which point the mathematical model begins to deviate from the experimental data.

Droplet removal due to wettability gradient Population balance model can also be adapted to model DWC with spontaneous drop removal due to wettability gradient, as shown by Singh et al.[24]. The DWC on a surface with wettability gradient differs from that on DWC on a uniform wettability inclined surface. In DWC on a surface with uniform wettability, coalescence of drops does not change the drop departure radius. However, in the case of DWC on a surface with wettability gradient, the coalescence of drops reduces drop size at which drops depart the surface. In the DWC on a surface with wettability gradient, the center of mass of the coalescing drops moves towards the high wetting region and the whole of the merged drop begins to move in the direction of the high wettability. The mathematical model of Singh et al. accounted for the effect of drop coalescence on drop departure radius. In the model, they calculated the drop departure size by balancing the hysteresis force by force due to wettability gradient and force generated by energy released during drop coalescence. Accounting for the effect of drop coalescence, the drop departure radius on a horizontal surface with wettability gradient is given by[24]

$$\pi {r_{\text{b}}}^2 \gamma \frac{\mathrm{d}(\cos\theta_{\text{d}})}{\mathrm{d}x} - \left(2\gamma r_b (\cos\theta_{\text{ro}} - \cos\theta_{\text{ao}}) - F_a \right) = 0. \quad (22)$$

here subscript o denotes the center of the base of the drop. In the above equation, the first term on

left-hand side represents force due to wettability gradient, the second term represents hysteresis force, and the third term denotes force due to the energy released during coalescence of two drops and is given by

$$F_a = \eta F_r, \tag{23}$$

where F_r and η are, respectively, given by

$$F_d = \frac{0.8\pi r_b \gamma_{lv}(2\,(1 - \cos\,\theta_d) - \sin^2\theta_d\,\cos\,\theta_d)}{\sin\,\theta_d}, \tag{24}$$

$$\eta = \frac{\Delta E - E_{vis}}{\Delta E}. \tag{25}$$

In Eq.(25) ΔE[42] and E_{vis}[43–45] are the energy released and viscous energy dissipated during coalescence of two identical sized drops. These are given by

$$E_{vis} = 144\mu\sqrt{\frac{r^3\gamma}{\rho}}\frac{(\theta_d + \sin\,\theta_d\,\cos\,\theta_d)^2}{\pi(2 - 3\,\cos\,\theta_d + \cos^3\theta_d)}, \tag{26}$$

$$\Delta E = \gamma\,\Delta A_{lv} - (\gamma\,\cos\,\theta_d)\,\Delta A_{sl}, \tag{27}$$

where, $\Delta A_{lv} = 0.82\,\pi r^2(1 - \cos\,\theta_d)$ and $\Delta A_{sl} = 0.41\,\pi r^2 \sin^2\theta_d$, respectively, are the change in the surface area of liquid vapor and solid–liquid interfaces.

Solution of Eq. (22) gives the drop departure radius r_{max} on a surface with wettability gradient using which the drop size distribution of large drops can be calculated using Eq. (15). Thereafter, similar to the approach used for inclined surfaces, the drop size distribution of small drops is obtained using Eqs. (19)–(21).

To model the surface with wettability gradient, the entire condensation surface is divided into m parts of equal width in the direction of wettability gradient. The variation in the contact angle is assumed to be of the form $\cos\theta = I + Sx$, where x is the spatial coordinate along the wettability gradient from low wetting to high wetting end. Then, the condensation heat flux through each segment is calculated using Eq. (1). After that, the heat transfer in each segment is numerically integrated to get the total dropwise condensation heat transfer. Singh et al.[24] validated their model by comparing the predictions of DWC heat flux and steady-state normalized population distribution of their model with the experimental results of Daniel et al.[21] and Macner et al.[22], respectively. Figures 11 and 12, respectively, shows the comparison of numerical predictions of the model with experimental results of Daniel et al. and Macner et al., respectively. The predictions of the mathematical model of Singh et al. agree well with the experimental results of Daniel et al. but only for the degree of subcooling less than 4 K. For the degree of subcooling greater than 4 K, the predictions of the model have a considerable deviation from the experimental results which the Singh et al. attributed to the beginning of transition regime. In transition regime, vapor condenses partially in filmwise form and partially in dropwise form.

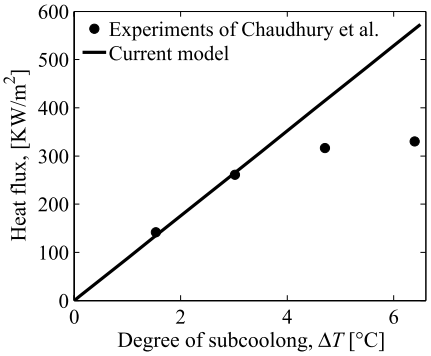

Figure 11: Comparison of heat flux predicted by mathematical model of by Singh et al. [24] with experimental data of Chaudhury et al. [46]. The calculations are based on nucleation site density, $N_s = 1 \times 10^{10}$ m^{-2}, $T_{sat} = 373$ K, $\delta = 100$ nm.

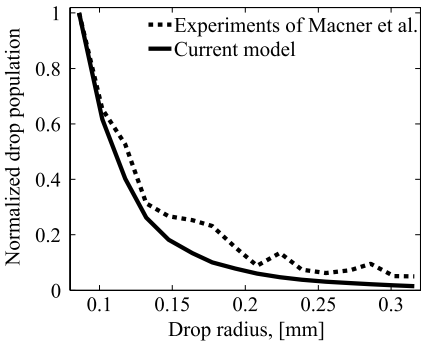

Figure 12: Comparison of population distribution predicted by mathematical model of Singh et al.[24] with experimental data of Macner et al.[22]. These calculations are performed for nucleation site density, $N_s = 1 \times 10^{10}$ m^{-2}, $T_{sat} = 373$ K, $\delta = 100$ nm. Reprinted from Singh et al. [24] Copyright 2018.

2.2.2 Monte Carlo Simulations

The population balance model is based on the assumption that the drop size distribution is in a statistically steady state. This steady state is attained when the drops removed from the condensation surface due to gravity or wettability

gradient are continuously replaced by the nucleation of new drops. However, dropwise condensation phenomena are an inherently unsteady process. Therefore, it is essential to understand the actual drop size distribution with time and their effect on the heat transfer coefficient. Due to the resolution limits in experiments, it is difficult to obtain the drop size distribution of small droplets. Hence, numerical simulations are used to predict drop size distribution. Solving Navier–Stokes equations for DWC are extremely challenging due to the difficulties associated with the tracking of interface position of the large number of condensing droplets. Moreover, such a simulation approach is computationally expensive. Therefore, the Monte Carlo method is commonly employed to simulate dropwise condensation. We divide this section into two parts: (i) simulations to study heat transfer and (ii) simulations to examine the pattern of droplets, known as Breath figures.

Heat transfer studies The first simulation model using Monte Carlo technique was proposed by Gose et al.[47]. Their model accounts for droplet nucleation, growth, coalescence, removal of a droplet from the surface, and re-nucleation on the exposed area. In this model, droplets are nucleated randomly on the condensing surface. At each time step, droplets grow due to direct condensation at the liquid–vapor interface. The rate of droplet growth is calculated using a equation similar to Eq. (14). When any two droplets touch or overlap, they coalesce to form a larger droplet. The resultant droplet is placed at the site of larger drop. When the droplet reaches a critical size, that is, when the gravity overcomes the surface tension force, the droplet is removed from the surface. The fresh condensation starts on the cleared area.

The results of Gose et al.[47] showed an order of magnitude lower heat transfer coefficient than the experimentally observed values because of lower initial nucleation site density ($10^4\,\mathrm{cm}^{-2}$). Later, Glicksman and Hunt[48] performed simulations by dividing the condensation cycle into four stages and taking the initial nucleation density of the order of $10^8 - 10^9\,\mathrm{cm}^{-2}$. Due to large initial density, their results were in good agreement with the experimental results. However, because of larger time step, the predicted droplet position and drop size distribution differed from the real behavior. Later, Burnside and Hadi[49] presented simulations of droplet growth from drop nucleation (≈ 17 nm) to a drop of about $4\,\mu\mathrm{m}$ which were difficult to observe through experiments. Figure 13 shows the evolution of drops in the central part of the condensing surface ($150\,\mu\mathrm{m} \times 150\,\mu\mathrm{m}$) for different instants of time. Their simulation results showed that Tanaka's[50] drop distribution theory which is given by $N \sim r^{-3}$ (where N is droplet density and r is drop size) is also valid for very small droplets.

The simulations were limited for hemispherical drops. Thereafter, Sikarwar et al.[51] extended the model to account for different contact angles of the surface. They observed that the saturation surface coverage decreases with the increase of contact angle. In addition, they performed simulation on inclined surfaces and reported that droplet fall-off time linearly decreases with the increase of contact angle.

Breath figure studies The pattern formed by the condensed droplets on the surface is commonly known as breath figure (BF). Several studies have been performed to understand the droplet growth pattern and their scaling laws during breath figure formation, beginning with Beysens and Knobler[52]. Beysens and Knobler were the first to identify different growth regimes on non-wetting surfaces. They reported that when the drops grow as an individual drop, it follows the power law $R \sim t^{\mu}$, where $\mu = 0.23$ and in the coalescence-dominated region (or self-similar regime), the average droplet grows with $R \sim t^{\mu_0}$, where $\mu_0 = 0.75$. Later, Viovy et al.[53] employed scaling analysis to study the dependence of growth law on the dimensionality of the condensing surface (D_s) and the droplet (D_d). Their results suggest that the growth law exponent $\mu = 1/D_d$ for a single droplet, whereas, $\mu_0 = 1/(D_d - D_s) = 3\mu$ for self-similar coalescence-dominated regime.

However, the transition of exponent from μ to μ_0. was difficult to observe through experiments. Furthermore, the evolution of the average droplet radius, surface coverage, polydispersity, and size distribution of drops with time was not clear. Therefore, Fritter et al.[54] developed a simulation model similar to Gose et al. and performed simulations for different initial surface coverages and polydispersities, and confirmed the growth law exponents. They observed the self-similar behavior described by a constant surface coverage of 0.57 in the coalescence dominated regime as shown in the inset plot of Fig 14. Furthermore, the size distribution of drops is bi-modal, because some of the drops do not undergo any coalescence events. Later, Steyer et al.[55] extended the same model for the growth of droplets on a one-dimensional surface. Their simulation results

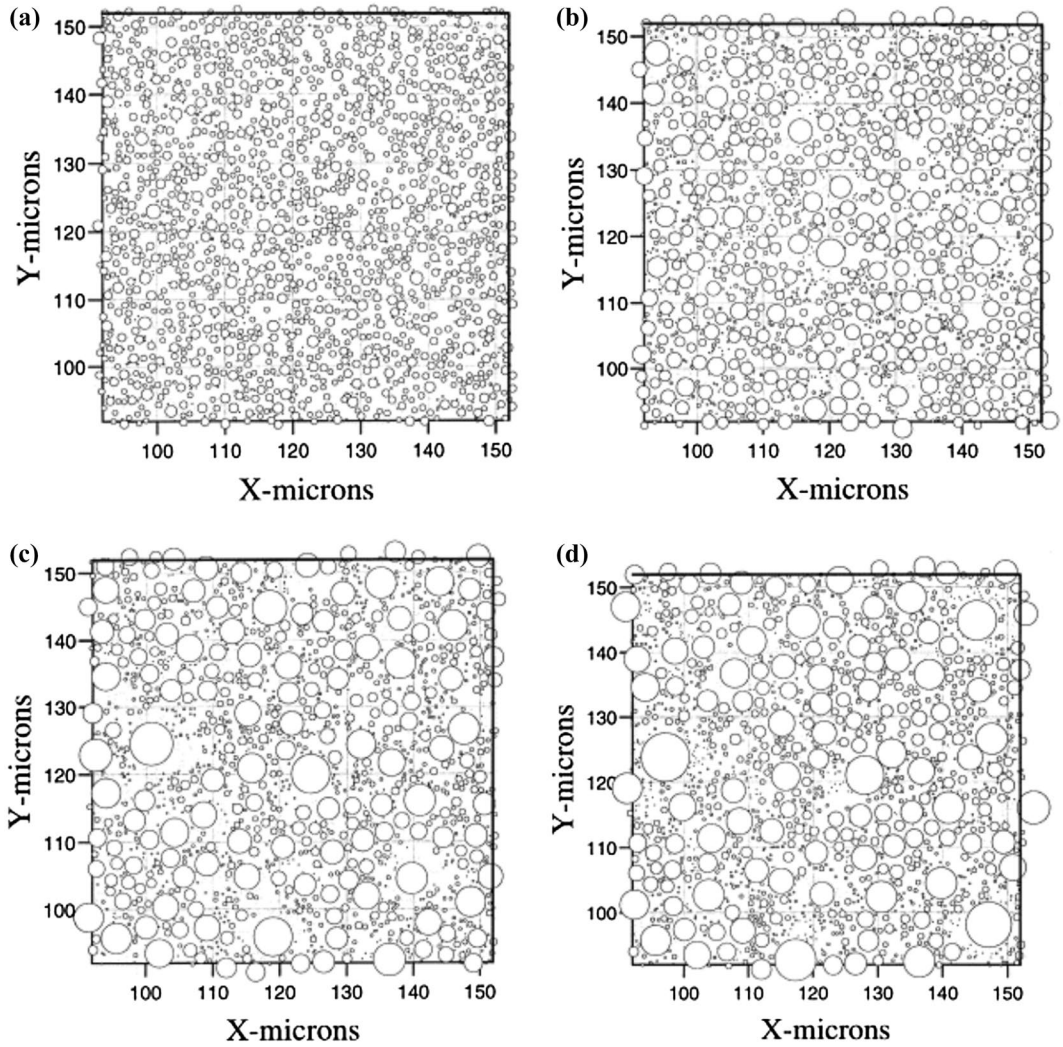

Figure 13: Evolution of drops in the central part of the condensing surface for different instants of time. **a** 0.007 ms, **b** 0.13 ms, **c** 0.19 ms, **d** 0.21 ms ($T_s = 373$ K, $\Delta T = 3$ K). Reprinted from Burnside and Hadi[49]. Copyright 1999, with permission from Elsevier.

show that for three-dimensional drops growing on a one-dimensional substrate, $\mu_0 = 3/2\mu$ in coalescence-dominated regime with the constant surface coverage of 0.8. Besides these Monte Carlo studies on DWC, various other Monte Carlo methods have been presented which take into account additional effects such as droplet growth due to diffusion[56,57] and jumping[58].

3 Conclusion

We have presented a comprehensive review and comparison of modeling techniques of dropwise condensation. We discussed the statistical approach used to model the inherently unsteady process of dropwise condensation. In the statistical approach, heat transfer through a single drop is combined with respective drop population to obtain the dropwise condensation heat transfer. Therefore, the statistical approach is divided into two parts (i) calculation of heat transfer through a single drop of radius r and (ii) prediction of drop size distribution. First, we discussed analytical model and simulation technique used to obtain the heat transfer through a single drop. We also presented a comparison between the analytical model and various simulation studies present in the literature. Next, we discussed the population balance model for prediction of drop size distribution in DWC. We have discussed the mathematical model for two cases where drop removal occurs due to (i) gravity and (ii) wettability gradient. Finally, we have presented a review of Monte Carlo methods for simulating DWC.

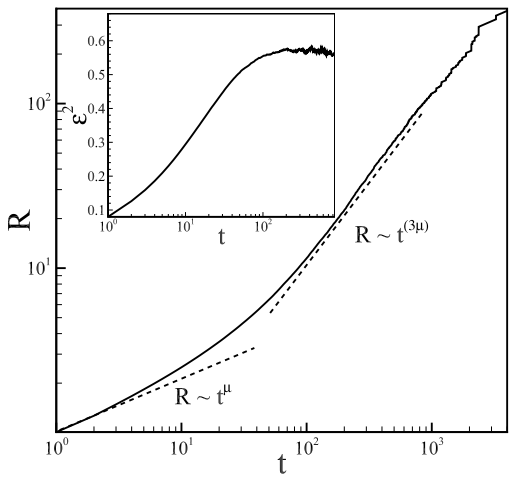

Figure 14: Evolution of average droplet radius ***R*** with time ***t*** and the inset plot shows the evolution of surface coverage ε^2 with time.

Publisher's Note

Springer Nature remains neutral with regard to jurisdictional claims in published maps and institutional affiliations

Received: 7 February 2019 Accepted: 14 February 2019
Published online: 4 March 2019

References

1. Ber JM (2007) High efficiency electric power generation: the environmental role. Prog Energy Combust Sci 33(2):107
2. Agency IE (2015) Key world energy statistics. International Energy Agency, Paris
3. Pérez-Lombard L, Ortiz J, Pout C (2008) A review on buildings energy consumption information. Energy Build 40(3):394
4. Humplik T, Lee J, O'Hern SC, Fellman BA, Baig MA, Hassan SF, Atieh MA, Rahman F, Laoui T, Karnik R, Wang EN (2011) Nanostructured materials for water desalination. Nanotechnology 22(29):292001
5. Cohen-Tanugi D, Grossman JC (2012) Water desalination across nanoporous graphene. Nano Lett 12(7):3602
6. Corry B (2008) Designing carbon nanotube membranes for efficient water desalination. J Phys Chem B 112(5):1427
7. Khawaji AD, Kutubkhanah IK, Wie JM (2008) Advances in seawater desalination technologies. Desalination 221(1):47
8. Andrews HG, Eccles EA, Schofield WCE, Badyal JPS (2011) Three-dimensional hierarchical structures for fog harvesting. Langmuir 27(7):3798
9. Lee A, Moon MW, Lim H, Kim WD, Kim HY (2012) Water harvest via dewing. Langmuir 28(27):10183
10. Schemenauer RS, Cereceda P (1991) Fog-water collection in arid coastal locations. Ambio 20(7):303–308
11. Leach RN, Stevens F, Langford SC, Dickinson JT (2006) Dropwise condensation: experiments and simulations of nucleation and growth of water drops in a cooling system. Langmuir 22(21):8864
12. Peters TB, McCarthy M, Allison J, Dominguez-Espinosa F, Jenicek D, Kariya H, Staats WL, Brisson JG, Lang JH, Wang EN (2012) Design of an integrated loop heat pipe air-cooled heat exchanger for high performance electronics. IEEE Trans Compon Packag Manuf Technol 2(10):1637
13 Kim MH, Bullard CW (2002) Air-side performance of brazed aluminum heat exchangers under dehumidifying conditions. Int J Refrig 25(7):924
14. Wen R, Ma X, Lee YC, Yang R (2018) Liquid-vapor phase-change heat transfer on functionalized nanowired surfaces and beyond. Joule 2(11):2307
15. Khandekar S, Muralidhar K (2014) Dropwise condensation on inclined textured surfaces. Springer, New York, NY (electronic resource)
16. Schmidt E, Schurig W, Sellschopp W (1930) Versuche über die Kondensation von Wasserdampf in Film- und Tropfenform. Tech Mech Thermodyn 1(2):53
17. Carey VP (2007) Liquid-vapor phase-change phenomena: an introduction to the thermophysics of vaporization and condensation process in heat transfer equipment. Taylor & Francis, New York, NY
18. Rose JW (2002) Dropwise condensation theory and experiment: a review. Proc Inst Mech Eng Part A 216(2):115
19. Tanasawa I, Utaka Y (1983) Measurement of condensation curves for dropwise condensation of steam at atmospheric pressure. J Heat Transf 105(3):633
20. Stylianou S, Rose J (1983) Drop-to-filmwise condensation transition: heat transfer measurements for ethanediol. Int J Heat Mass Transf 26(5):747
21. Daniel S, Chaudhury MK, Chen JC (2001) Fast drop movements resulting from the phase change on a gradient surface. Science 291(5504):633
22. Macner AM, Daniel S, Steen PH (2014) Condensation on surface energy gradient shifts drop size distribution toward small drops. Langmuir 30(7):1788
23. Singh M, Kondaraju S, Bahga SS (2017) Enhancement of thermal performance of micro heat pipes using wettability gradients. Int J Heat Mass Transf 104:400
24. Singh M, Kondaraju S, Bahga SS (2018) Mathematical model for dropwise condensation on a surface with wettability gradient. J Heat Transf 140:071502
25. Vemuri S, Kim K, Wood B, Govindaraju S, Bell T (2006) Long term testing for dropwise condensation using self-assembled monolayer coatings of n-octadecyl mercaptan. Appl Therm Eng 26(4):421
26. Enright R, Miljkovic N, Alvarado JL, Kim K, Rose JW (2014) Dropwise condensation on micro- and

nanostructured surfaces. Nanoscale Microscale Thermophys Eng 18(3):223
27. Cho HJ, Preston DJ, Zhu Y, Wang EN (2017) Nanoengineered materials for liquid-vapour phase-change heat transfer. Nat Rev Mater 2(2):16092
28. Tanaka H (1975) A theoretical study of dropwise condensation. J Heat Transf 97(1):72
29. Kim S, Kim KJ (2011) Dropwise condensation modeling suitable for superhydrophobic surfaces. J Heat Transf 133(8):081502
30. Ranodolph A (2012) Theory of particulate processes 2e: analysis and techniques of continuous crystallization. Elsevier, California, CA
31. LeFevre E, Rose J (1966) A theory of heat transfer by dropwise condensation. In: Proceedings of the third international heat transfer conference, vol. 2 (Chicago, IL), vol. 2, pp 362 – 375
32. Savino R, Fico S (2004) Transient Marangoni convection in hanging evaporating drops. Phys Fluids 16(10):3738
33. Guadarrama-Cetina J, Narhe RD, Beysens DA, González-Viñas W (2014) Droplet pattern and condensation gradient around a humidity sink. Phys Rev E 89:012402
34. Chavan S, Cha H, Orejon D, Nawaz K, Singla N, Yeung YF, Park D, Kang DH, Chang Y, Takata Y, Miljkovic N (2016) Heat transfer through a condensate droplet on hydrophobic and nanostructured superhydrophobic surfaces. Langmuir 32(31):7774
35. Phadnis A, Rykaczewski K (2017) The effect of Marangoni convection on heat transfer during dropwise condensation on hydrophobic and omniphobic surfaces. Int J Heat Mass Transf 115:148
36. Rykaczewski K (2012) Microdroplet growth mechanism during water condensation on superhydrophobic surfaces. Langmuir 28(20):7720
37. Xu Z, Zhang L, Wilke K, Wang EN (2018) Multiscale dynamic growth and energy transport of droplets during condensation. Langmuir 34(30):9085
38. Maa JR (1978) Drop size distribution and heat flux of dropwise condensation. Chem Eng J 16(3):171
39. Abu-Orabi M (1998) Modeling of heat transfer in dropwise condensation. Int J Heat Mass Transf 41(1):81
40. Daniel S, Chaudhury MK (2002) Rectified motion of liquid drops on gradient surfaces induced by vibration. Langmuir 18(9):3404
41. Vemuri S, Kim K (2006) An experimental and theoretical study on the concept of dropwise condensation. Int J Heat Mass Transf 49(3–4):649
42. De Gennes PG, Brochard-Wyart F, Quéré D (2013) Capillarity and wetting phenomena: drops, bubbles, pearls, waves. Springer-Verlag, New York, NY
43. Chandra S, Avedisian C (1991) On the collision of a droplet with a solid surface. In: Proceedings of the royal society of london a: mathematical, physical and engineering sciences, vol. 432 (The Royal Society), vol. 432, pp 13–41
44. Wang FC, Yang F, Zhao YP (2011) Size effect on the coalescence-induced self-propelled droplet. Appl Phys Lett 98(5):053112
45. Lv C, Hao P, Yao Z, Song Y, Zhang X, He F (2013) Condensation and jumping relay of droplets on lotus leaf. Appl Phys Lett 103(2):021601
46. Chaudhury MK, Chakrabarti A, Daniel S (2015) Generation of motion of drops with interfacial contact. Langmuir 31(34):9266
47. Gose EE, Mucciardi A, Baer E (1967) Model for dropwise condensation on randomly distributed sites. Int J Heat Mass Transf 10(1):15
48. Glicksman LR, Hunt AW (1972) Numerical simulation of dropwise condensation. Int J Heat Mass Transf 15(11):2251
49. Burnside B, Hadi H (1999) Digital computer simulation of dropwise condensation from equilibrium droplet to detectable size. Int J Heat Mass Transf 42(16):3137
50. Tanaka H (1975) Measurements of drop-size distributions during transient dropwise condensation. J Heat Mass Transf 97(3):341
51. Sikarwar BS, Battoo NK, Khandekar S, Muralidhar K (2011) Dropwise condensation underneath chemically textured surfaces: simulation and experiments. J Heat Mass Transf 133(2):021501
52. Beysens D, Knobler CM (1986) Growth of breath figures. Phys Rev Lett 57:1433
53. Viovy JL, Beysens D, Knobler CM (1988) Scaling description for the growth of condensation patterns on surfaces. Phys Rev A 37:4965
54. Fritter D, Knobler CM, Roux D, Beysens D (1988) Computer simulations of the growth of breath figures. J Stat Phys 52(5):1447
55. Steyer A, Guenoun P, Beysens D, Fritter D, Knobler CM (1990) Growth of droplets on a one-dimensional surface: experiments and simulation. Europhys Lett (EPL) 12(3):211
56. Steyer A, Guenoun P, Beysens D, Knobler CM (1991) Growth of droplets on a substrate by diffusion and coalescence. Phys Rev A 44:8271
57. Meakin P (1992) Dropwise condensation: the deposition growth and coalescence of fluid droplets. Phys Scr T44:31
58. Narhe RD, Khandkar MD, Shelke PB, Limaye AV, Beysens DA (2009) Condensation-induced jumping water drops. Phys Rev E 80:031604

Manjinder Singh is a PhD student at Indian Institute of Technology Delhi. He received his M. Tech from National Institute of Technology Jalandhar in 2013. His research at IIT Delhi focuses on micro-heat pipes based on wettability gradient.

Nilesh D. Pawar is a Ph.D. student at Indian Institute of Technology Delhi. He received his M. Tech from Indian Institute of Technology Kharagpur in 2013. His research at IIT Delhi focuses on droplet condensation and lattice Boltzmann simulations.

Sasidhar Kondaraju is an Assistant Professor in the School of Mechanical Sciences at Indian Institute of Technology Bhubaneswar. He received his bachelor's degree from Osmania University, Hyderabad, India in 2003 and received his M.S. and Ph.D. degrees from Wayne State University, Detroit, USA in 2006 and 2009, respectively. His research interests include investigation of fundamental mechanisms for interfacial fluid mechanics, droplet microfluidics, and droplet evaporation and condensation. He has published 23 articles in international journals.

Supreet Singh Bahga is an Assistant Professor in the Department of Mechanical Engineering at Indian Institute of Technology Delhi. He received his B. Tech. in Mechanical Engineering from Indian Institute of Technology Bombay in 2007, and M.S. and Ph.D. in Mechanical Engineering from Stanford University in 2009 and 2013, respectively. His research interests include theoretical and experimental investigation of micro-scale transport phenomena. He has co-authored 28 articles in international journals.